UNPARALLELED COUPLED OCEAN-ATMOSPHERE SUMMER HEATWAVES IN THE NEW ZEALAND REGION: DRIVERS, MECHANISMS AND IMPACTS

M James Salinger[1], Howard J Diamond[2], Erik Behrens[3], Denise Fernandez[3], B Blair Fitzharris[4], Nicholas Herold[5], Paul Johnstone[6], Huub Kerckhoffs[7], A Brett Mullan[3], Amber K Parker[8], James Renwick[9], Claire Schofield[6], Allan Siano[7], Robert O Smith[10], Paul M South[11], Phil J Sutton[3,12], Edmar Teixeira[6], Mads S Thomsen[13] and Michael C T Trought[14]

1. [1] Department Agriculture, Food, Environment and Forestry (DAGRI), University of Florence, Florence 50144, Italy Orchid id: 0000-0002-5782-1411

[2] NOAA/Air Resources Laboratory, College Park, Maryland 20740, USA

[3] National Institute of Water and Atmospheric Research, Wellington, New Zealand

[4] Department of Geography, University of Otago, Dunedin, New Zealand

[5] The NSW Department of Planning, Industry and Environment, Science Division, Climate and Atmospheric Science, New South Wales, Australia. Geography, Environment & Earth Sciences, Victoria University of Wellington, Wellington New Zealand

[6] New Zealand Institute for Plant and Food Research Limited, New Zealand

[7] School of Agriculture and Environment, Massey University, Palmerston North, New Zealand

[8] Department of Wine, Food and Molecular Biosciences, Lincoln University, New Zealand

[9] School of Geography, Environment & Earth Sciences, Victoria University of Wellington, Wellington New Zealand

[10] Department of Marine Science, University of Otago, Dunedin, New Zealand

[11] Cawthron Institute, Nelson, New Zealand

[12] School of Environment, University of Auckland, Auckland, New Zealand

[13] Centre of Integrative Ecology and the Marine Ecology Research Group, School of Biological Sciences, University of Canterbury, Christchurch, New Zealand

[14] Innovative Winegrowing, Blenheim, New Zealand

* Corresponding author: M. James Salinger, jimbosalinger@gmail.com, + 64 21 221 9461

Abstract

During austral summers (DJF) 1934/35, 2017/18 and 2018/19, the New Zealand (NZ) region experienced the most intense coupled ocean-atmosphere heatwaves covering an area of approximately 4 million km^2 in each case. Average air temperature anomalies over land were +1.7 to 2.1°C above average while sea surface temperatures (SST) were 1.2 to 1.9°C above average. All three heatwaves exhibiting maximum SST anomalies to the west of the South Island of NZ. Atmospheric circulation anomalies show a pattern of strong blocking centred over the Tasman Sea and extending south-east of NZ, accompanied by positive Southern Annular Mode conditions, and reduced trough activity over NZ. Rapid melt of seasonal snow occurred in all three cases. For the two most recent events, very shallow anomalies of sub-surface ocean temperature were observed. Ice loss in the Southern Alps was estimated at 7.0 km^3 water equivalents (w.e.) (17% of the 2017 volume) Sauvignon blanc and Pinot noir wine grapes had above average berry number and bunch mass in 2018 but were below average in 2019. Summerfruit (cherries and apricots) were 14 and 2 days ahead of normal in 2017/18 and 2018/19 respectively. Spring wheat simulations suggested earlier flowering and lower grain yields compared to average, and below-average yield and tuber quality in potatoes crops occurred. Major species disruption occurred in marine ecosystems. Hindcasts indicate the heatwaves were either atmospherically driven or arose from combinations of atmospheric surface warming and oceanic heat advection.

Keywords: Anthropogenic global warming, marine heatwave, atmospheric heatwave, terrestrial ecosystems, marine ecosystems, crops, human health.

1. Introduction

Kidson (1935) described the first documented austral summer (DJF) heatwave covering the New Zealand (NZ) area in 1934/35, with regional temperatures anomalies over land being +1.7ºC relative to the 1981-2010 normal. At the time this event was so unusual being almost 3ºC warmer than other summers in the 1930s that it was described as “remarkably warm”. Salinger et al (2019a) documented the unprecedented austral summer (DJF) 2017/18 heatwave covering the NZ region. Regional average air (over land) and sea surface temperature anomalies were +2.2ºC and +1.9ºC, respectively. This event had numerous terrestrial and marine impacts and persisted for the entire austral summer resulting in the (1) largest loss of glacier ice in the Southern Alps since 1962; (2) early sauvignon blanc wine-grape maturation; and (3) major species disruption in marine ecosystems. Various atmospheric drivers were identified, and the event was associated with very low wind speeds, reduced upper ocean mixing and heat fluxes from the atmosphere to the ocean causing substantial warming of the stratified surface layers of the Tasman Sea.

Using the Hobday et al (2016) definition of marine heat waves (MHW), Oliver et al (2018) found a 54% increase in the number of MHW days globally since the early 20th century with an increase of 0.3-0.9 days per year in the NZ region. From two General Circulation Model (GCM) ensembles, Perkins-Kirkpatrick et al (2018) concluded that a Tasman Sea MHW with the intensity of the 2017/18 event would have been virtually impossible without anthropogenic forcing. The atmospheric blocking that was responsible for the prolonged period of high mean sea level pressure (MSLP) also displayed some anthropogenic influence.

MHWs are caused by a range of processes operating across different spatial and temporal scales, from localized air–sea heat flux to large-scale climate drivers, such as the El Niño Southern Oscillation (ENSO; Heidemann and Ribbe, 2019) and Southern Annular Mode (SAM; Thompson et al, 2011). Behrens et al (2019) investigated mechanisms of MHWs in the

Tasman Sea using data from a forced global sea-ice model and from Argo observations to conclude that they are largely controlled by meridional heat transport from the subtropics through the interchange between the East Australian Current and the Tasman Front. One contributor to the increased frequency of MHWs (Oliver et al, 2018) has been regional warming trends. Sutton and Bowen (2019) documented a 0.1 to 0.3°C per decade increase since 1981 in ocean temperatures with the warming penetrating from the surface to 200m depth around coastal NZ and to at least 850m in the eastern Tasman Sea.

This study examines the three most intense atmospheric heatwaves (AHW) and associated MHW for the NZ region covering the austral summer heatwaves of 1934/35, 2017/18 and 2018/19. It diagnoses the atmospheric and oceanic drivers, impacts on terrestrial and marine ecosystems, including viticulture and arable cropping. Monthly to decadal atmospheric and oceanic mechanisms were investigated, along with an an assessment of future likelihood of similar repeat events.

1. Methods

Many of the methods used here were described in Salinger et al (2019a). They are outlined briefly here, with new approaches described in more detail.

2.1 Observations of atmosphere and ocean temperature, and diagnostics

The 22-station NZ air temperature (NZ22T) series (Salinger et al 1992) was used to calculate monthly mean air temperature anomalies for the period 1940-2018, relative to the 1981-2010 normal. From daily time series, extreme statistics TX90p (percentage of days when the daily maximum temperature is above the 90th percentile), TN90p (percentage of days when the daily minimum temperature is above the 90th percentile), and number of summer days ≥25°C were calculated as in Salinger et al (2019a). Eight stations were analysed for the 1934/35 event. Monthly sea surface temperature (SST) observations were obtained from Extended Reconstructed Sea Surface Temperature version 5 (ERSST) as in Salinger et al (2019a).

For the NZ exclusive economic zone (NZEEZ, an area of around 4 million km^2), an area-weighted temperature anomaly was calculated from SST and land surface temperatures. The 2°×2° ERSST product from 34 to 48°S, and 165° to 179°E was combined with NZ22T to produce a new temperature series: the NZEEZT series.

Daily SST estimates were obtained from the NOAA ¼° daily Optimum Interpolation SST analysis (daily OISST) on a 0.25° latitude/longitude grid spanning September 1981-July 2019 as in Salinger et al (2019a). These were averaged over the region 160-172°E and 35-45°S. Daily 9 am measurements of SST since 1953 were obtained at the Portobello Marine Laboratory (PML) in Otago Harbour, South Island, NZ. The Hobday et al (2016; 2018) MHW definitions were applied to identify and characterise MHWs based on daily SST measurements from the daily OISST and PML datasets as in Salinger et al (2019a). Ocean sub-surface temperature from GODAS data (Saha et al, 2006) were averaged between 40°S and 45°S, 140°E and 150°W, over the depth range 25 to 600m, and Argo profiles (Jayne et al, 2017) were extracted for the eastern Tasman Sea (160-172°E, 35-45°S), as in Salinger et al (2019a).

For atmospheric circulation, monthly mean sea level pressure (MSLP) and 500-hPa geopotential height fields were obtained (Salinger et al 2019a) from the NCEP/NCAR Reanalysis (Kistler et al, 2001) and from the ERA-Interim reanalysis (Dee et al, 2011). Several indices were used to characterize the circulation: Trenberth (1976) Z1 and M1 indices as well as weather regimes over NZ (Kidson 2000) for the last two compared with the 1981- 2010 normal. For large-scale circulation and monthly to decadal modes of variability the following were used: the Gong and Wang (1999) Southern Annular Mode (SAM) index, the Southern Oscillation Index (SOI) of Troup (1965), and for the Interdecadal Pacific Oscillation (IPO) the tripolar index (Henley et al 2015).

A subset of past analogue (similar) three-month periods was chosen from both the ERA-Interim and 20^{th} Century reanalysis (20CR, Compo et al, 2011). Analogues were selected for each of the three summers based on anomaly correlation and root mean-squared difference (RMSD) using 500hPa anomaly fields over the NZ/Tasman Sea region. Analogues that exhibited anomaly correlations of at least 0.65 and RMSD of 19 geopotential metres (gpm) or less were selected. For 1934/35, the RMSD threshold was reduced to 16 gpm to reduce the number of analogue cases to a comparable level to the later summers A total of eight 20CR analogues were chosen for 1934/35, while 11 and 10 ERA-Interim analogues were chosen for 2017/18 and 2018/19 respectively.

The global ocean model hindcast for this study was as described in Salinger et al (2019a). The climatology over the period 2000 to 2018 was used to remove the seasonal signal. Heat content anomalies were computed over the mixed layer depth, which is defined by a density difference of 0.01 kg/m^3 from the surface.

2.2 Snow and ice data

The end of summer snowline (EOSS) time series (Chinn et al 2012) was used to estimate Southern Alps mountain glacier mass balance from 1977 to 2018 for $EOSS_{Alps}$ (Salinger et al 2019a). Regression relationships were employed to calculate values of $EOSS_{Alps}$ for 1935 and 2019, using Hermitage Mt Cook glacier season annual mean temperature, the SAM index, and Kidson (2000) Trough and Block regimes frequencies (Salinger et al (2019b). $EOSS_{Brewster}$ was estimated from satellite imagery and regression relations between $EOSS_{Alps}$ and $EOSS_{Brewster}$ to derive a value for 2019. The methods of Chinn et al (2012) were used to estimate downwasting (continuous decrease in the level of a glacier in the net melting zone) and proglacial lake growth.

Estimates of water stored as seasonal snow in the South Island for 2017-18 and 2018-19 were provided by a conceptual model (SnowSim), available through Meridian Energy Ltd (*https://www.meridianenergy.co.nz/who-we-are/our-power-stations/snow-storage/*) (Garr and Fitzharris 1996). The SnowSim model calculates water stored as seasonal snow for key hydrogenerating river catchments and is tuned to their long-term water balance. Past estimates are in general agreement with historical observations of snow back to 1930. Estimates for seasonal snow for 1934-35 are given in Fitzharris and Garr (1995) and de Lautour (1999).

2.3 Agriculture

2.3.1 Horticulture

Grapes

The impact of grapevine phenology was predicted using the Grapevine Flowering Véraison (GFV) model (Parker et al 2013) and the harvest model (defined as a sugar concentration of 200 g/L; Parker 2012). Meteorological data were sourced from the Marlborough Regional Station (41.48^{o}S; 173.95^{o}E). Observations of yield component data over 10 seasons were obtained from Marlborough commercial vineyards (Pinot noir n=13; Sauvignon blanc n=34). Inflorescence numbers per metre of row were collected shortly after budburst in November and bunch and berry mass shortly before harvest. Berry number per bunch was calculated from bunch and berry mass data.

Summer Fruit

Harvest dates were gathered for one variety of cherry (‘Lapins’) and two varieties of apricots (‘Nzsummer 2’ and ‘Nzsummer3’) at the Plant and Food Research orchard in Clyde, Central Otago (40.90°S 174.89°E) for 2016-2019, where meteorological data were also obtained.

2.3.2 Arable

Wheat

The Agricultural Production Systems sIMulator (APSIM; Holzworth et al 2014) was used to assess the performance of spring wheat during the three very hot summers (1934/35, 2017/18 and 2018/19) against long term historical climate (1981-2010). Simulations were set for a key wheat-producing area (Lincoln, Canterbury; 43.62°S 172.47°E) by assuming that crops were fully irrigated and fertilized to minimize the effects of additional yield-limiting factors in the assessment. The production metrics considered were flowering time, cycle length, grain yield and frequency of heat stress events during the reproductive period, when wheat crops are sensitive to yield-damage by short periods above threshold temperatures (Supplementary Material). No crop data are available.

Potatoes

A preliminary study sought early evidence of how the 2017/18 heatwave affected potato production in NZ (Siano et al 2018) at three sites: Ohakune in the central North Island (39.50°S, 175.45°E; 563 metres above sea level (masl)) which was irrigated, Opiki, south west North Island (40.46°S, 175.48°E; 4 masl) which was rainfed, and Hastings, eastern North Island (39.62°S, 176.73°E; 8 masl) which was irrigated. For the 2018/19 season, two locally bred (Ilam Hardy and Rua), and five offshore bred (Agria, Hermes, Taurus, Snowden and Fianna) processing cultivars were trialed at the three sites. The crops were established in 100 m^2 of land. Physiological data (net photosynthesis, transpiration rate and stomatal conductance) were measured at specific growth stages of the crop, while yield and tuber quality data were determined at final harvest.

2.4 Marine ecosystems

Impacts on marine ecosystems were evaluated from anecdotal observations together with published data describing immediate losses of bull kelp (*Durvillaea*) and associated community-change, and new data describing recovery of *Durvillaea* and its community 1.5 years after the MHW. Anecdotal information was obtained by searching for MHWs and changes to marine species in news outlets. Impacts on *Durvillaea* and its community were estimated by comparing drone images and detailed abundance-surveys of benthic species, respectively, before and after 2017/18 MHW. An experiment initiated in June 2017 was re-sampled in August 2019 to provide new data on *Durvillaea* recovery and community change (see Thomsen et al 2019 and Thomsen & South 2019 for details). New before/after MHW/*Duvillaea*-loss abundance-data for canopy-forming seaweeds at Pile Bay are shown.

3 Results

3.1 Observations of the atmosphere and oceans.

3.1.1 Surface temperatures

The coupled ocean-atmosphere heatwaves in the NZ region during the three austral summer seasons studied here were the most intense recorded in the NZ and Tasman Sea regions in 150 years of land-surface air temperature records, and ~40 years of satellite-derived SST records (Sutton 2019), as shown in Fig. 1a-f.

For all three heatwaves both land and sea surface air temperatures were 1.2° to 1.5°C above 1981-2010 averages over the entire region, from 32° to 52ºS, 150°E to 180º (Table 1 and Fig. 1). NZ22T anomalies (Table 1) were 1.7ºC, 2.1°C and 1.2ºC above average (Fig. 1a and Table 1), by far the three warmest on record (Salinger 1979, Mullan et al 2010). Indices of temperature extremes for NZ (Table 1 and Fig. 1b) show the highest percentage of summer warm days and warm nights above the 90th percentile (1934/35 26 and 26%, 2017/18 33 and 29% and 2018/19 22 and 17%) back to 1934. Counts of summer days ≥25ºC averaged 22, 32 and 26 days nationwide respectively for the three seasons.

For the Tasman Sea and east of NZ (32º–52°S, 150º–180°E) the MHWs were characterised by SSTs 1.5°C, 1.9°C and 1.2 above average (Figs. 1d-f), the largest anomalies on record. All three temperature anomalies showed a similar spatial pattern with highest anomalies to the west of the South Island of NZ. The major departures from average occurred in DJF for 1934/35 and 2017/18 but in JFM for 2018/19.

Applying a MHW definition (Hobday et al 2016) to the daily OISST for the eastern Tasman Sea (Fig. 2a) indicates that the summer 2018/19 event had a similar duration but reduced intensity compared to the 2017/18 event. During summer 2017/18, the eastern Tasman Sea experienced MHW conditions for 138 d (consisting of two distinct periods of 99 d and 39 d), peaking as a Category IV (Extreme) MHW (Hobday et al, 2018) with a maximum intensity of 4.1°C. In comparison, the 2018/19 event lasted for 137 d, peaking as a Category II (Strong) MHW, with a maximum intensity of 2.8°C. Nearshore surface waters at the PML followed a similar pattern during summer 2017/18 and 2018/19 (Fig. 2b), experiencing MHW conditions for several short (7-28 d) periods interspersed with cooler breaks. However, maximum intensities during summer 2018/19 (2.6°C) were approximately half those observed during summer 2017/18 (5.7°C) (Salinger et al 2019a).

3.1.2 Atmospheric circulation

Atmospheric circulation anomalies for the three DJF seasons (Fig. 3a-c) show a pattern of blocking (higher than normal pressures): 1934/35 and 2017/18 were to the east and southeast of NZ, with negative pressure anomalies northwest of NZ whereas the 2018/19 season had the strongest positive pressure anomalies over the central Tasman Sea. The M1 and Z1 circulation indices show significant northerly airflow for 1934/35, and easterly airflow for 1934/35 and 2017/18. Airflow was northeasterly for 2018/19. Kidson weather regimes show a lack of trough types in late spring (NDJ) together with lack of zonal regimes and more blocking throughout the season for 2017/18. In contrast 2018/19 had fewer blocking regimes, but more of the zonal regime.

The 500-hPa geopotential height anomalies were consistent (Fig. 3d-f) with very strong blocking in the Tasman Sea extending southeast of NZ. The 1934/35 had an average positive height anomaly of 30 gpm west of the North Island over the north Tasman Sea. The 2017/18 anomaly was the most intense, being 60 gpm to the south east of the South Island, whereas the 2018/19 anomaly was 40 gpm over the western Tasman Sea. The 1934/35 and 2018/19 events all exhibited ridges east and south east of the South Island.

Over austral spring and summer 1934/35 the SAM was negative, signalling an expanded circumpolar westerly vortex (Table 1). For 2017/18 the SAM was significantly positive throughout indicating a much-contracted vortex towards Antarctica, and for 2018/19 it was also positive. In 1934/35 the Troup SOI was near neutral with a value of -1.0. In 2017/18 ENSO was in a weak La Niña phase with an average SOI value of +0.7, and within the La Niña phase (+0.74) for 2018/19. This would on average be associated with northerly quarter airflow anomalies in spring, and north easterly airflow anomalies over NZ in summer (Gordon 1986). Only in the 2017/18 summer was the Interdecadal Pacific Oscillation index negative, enhancing any La Niña state.

3.1.3 Analogue seasons

The strength of the DJF 1934/35 anticyclone had an anomaly maximum of 30 gpm northwest of NZ (Fig 3d). The positive anomalies covered a wide area across most of NZ and, from the east coast of NZ to 155ºW at an average of about 10 gpm. The position (northwest of NZ as opposed to the southeast), extent, and intensity of this anticyclone was less than that for DJF 2017/18 season (Fig 3e, Salinger et al 2019a). Compared with the analogue cases in Table 2a, DJF 1934/35 was the 4th lowest SAM value in the group of 20CR seasons. The DJF 1934/35 SAM value (-1.21) was not statistically significant. Therefore, unlike the very strong statistically significant SAM value of +1.76 for the DJF 2017/18 season (Salinger et al 2019a), this negative SAM value is likely one reason, together with the position, intensity, and extent of the anticyclone, that the DJF 1934/35 season did not experience the same record warm levels as DJF 2017/18.

The DJF 2018/19 (Fig 3f) anticyclone anomaly reached a maximum of +40 gpm centred northwest of NZ. The position northwest of NZ (as opposed to southeast), extent, and intensity of this anticyclone was considerably less than was in place during DJF 2017/18 (Salinger et al 2019a). The SAM value (+0.36) for DJF 2018/19, while positive, was not statistically significant. Therefore, unlike the very strong statistically significant SAM value for DJF 2017/18, this lower SAM value of +0.36 likely is one reason, coupled with the position, intensity, and extent of the anticyclone, that DJF 2018/19 did not experience the same record warm levels as the previous 2017/18 season. However, in contrast the SOI of +0.74 was highly significant, which would on average have been associated with warm SST anomalies in the Tasman Sea. For 2017/18, blocking weather types (Kidson 2000) were most prevalent with lack of the zonal regime and the analogue seasons displayed a dominance of the blocking regime. In comparison 2018/19 zonal types were prevalent. In both cases, analogues exhibited a lack of the troughing regime.

3.1.4 Ocean Sub-Surface Temperature

The GODAS sub-surface ocean temperature patterns for DJF 2017/18 and 2018/19 for 40-45ºS (Fig. 4) indicate very shallow anomalies west of the South Island, with a narrow band down to about 50m east of the South Island. Anomalies also exist in the western Tasman Sea and into the south Pacific east of NZ. These were also shallow but far more intense in 2018/19 than in 2017/18. The Argo float measurements (Fig. 4c) averaged over the eastern Tasman Sea confirmed surface warming from December to February, peaking at 3ºC mean anomaly in 2017/18 and 1.5ºC in 2018/19. The warming anomaly then abated. The anomaly was shallow, mainly confined to the upper 20m when it formed, and both deepened slightly as they were eroded from the surface.

3.1.5 Ocean hindcasts

The MHW in 2015/16 which affected the region east of Tasmania (Fig. 5a) was documented by Oliver et al (2017) and attributed to enhanced heat transport of the East Australian Current Extension (EAC-Ext). The modelled SST anomalies are intensified south of 35ºS along the east coast of Australia and Tasmania and exceeded 1°C above the climatological mean. Positive SST anomalies are also present in the Tasman Front region, while the remaining Tasman Sea is characterised by negative SST anomalies, reaching from the southern tip of Tasmania to the North Cape of NZ. Mixed layer heat content anomalies show a pattern consistent with the SST anomalies, along the flow path of the EAC-Ext. where summer mixed layers are around 20m deep. In comparison to the 2015/16 event, the 2017/18 heat wave was more intense, with SST anomalies above 2ºC over large parts of the Tasman Sea. The mixed layer heat content anomaly was positive over the entire Tasman Sea but showed a different spatial pattern compared to the SST anomalies, which implies differences in the driving mechanism compared to the 2015/16 MHW. The 2017/18 event was predominantly atmospherically driven, with low wind speeds reducing the vertical mixing of heat into the water column and causing a shallow but intense surface warming. As the surface layer warmed, the mixed layers became shallower, and mixed layer heat content anomalies were reduced. This differs from cases where oceanic heat advection is dominant and mixed layer remain shallow, as in the case of the 2015/16 and 2018/19 MHW where SST and mixed layer heat content anomalies show similar patterns. The warming in 2018/19 extended from the EAC-Ext. region over the Southern Tasman Sea to the coastal waters of eastern NZ, and along the Chatham Rise. Each MHW event is affected by a combination of both surface warming and oceanic heat advection drivers (Behrens et al 2019), making each MHW unique.

SSTs, mixed layer heat content and winds speed anomalies vary on an annual basis over the Tasman Sea (Fig. 5g). While the period from 2003 to 2012 was predominantly characterised with negative mixed layer heat content anomalies and negative SSTs, the tendency has changed to more positive anomalies since then. The positive wind anomalies in 2014, 2015, 2016 with increased vertical mixing prevented the development of significant SST anomalies during spring.

3.2 Terrestrial ice and snow

3.2.1 Cryosphere

The ice volume loss in the Southern Alps for the small and medium glaciers was estimated to be 3.2 km^3 water equivalent (w.e.) in 1934/35, 3.6 km^3 in 2017/18 and 2.5 km^3 in 2018/19. This was 9.6 km^3 w.e. for the three heatwave summers, representing an 18% loss of the total ice volume of the Southern Alps, compared with the 1977 inventory (Chinn, 2001). For the two consecutive heatwave summers losses amounted to 6.1 km^3 w.e. Total ice loss (small and medium plus 12 large glaciers) came to 7.0 km^3 w.e. or an accumulated 17% of the 2017 volume, the largest for any period from 1962 (Fig. 6a).

3.2.2 Seasonal Snow

The 1934-1935 snow year was remarkable. Water stored as seasonal snow reached a maximum that was just below average at 402 mm w.e. in mid-October. Rapid snowmelt began in mid-November and such was the summer heat, all snow had disappeared by 11 January, the third earliest since 1930 (de Latour 1999). Melt rate over this period was 6.5 mm/d w.e., the highest of the three summers. The earliest date for disappearance of all seasonal snow is 28 December for the 1974-75 snow year, but this was from a maximum of only 198 mm w.e., amongst the lowest since 1930.

During the 2017-18 snow year, the estimated water stored as seasonal snow leading up to August (Fig. 6b) was very low. It reached a maximum of 30% of average at 350 mm w.e. in late September, much earlier than usual. However, rapid melt did not begin until 18 November and from mid-December 2018 the snowpack was the lowest on record. By 10 January all the seasonal snow had melted, the second earliest date for seasonal snow to disappear since 1930, with extraordinary loss of permanent glacier snow and ice. Melt rate over this period was 5.7 mm/d w.e.

The SnowSim model showed that maximum accumulation for the 2018-19 snow year was close to average at 420 mm w.e. and occurred in late October (Fig 6c), slightly later than normal. There was rapid melt from late November, but it took until 12 February for all the seasonal snow to disappear. Melt rate over this period was 5.0 mm/d w.e.

3.3 Agriculture

3.3.1 Horticulture

Grapes

Temperatures were above the long-term average for the 2017-18 and 2018-19 seasons. (Table 1: supplementary Figure S1) particularly at the key phenological stages of inflorescence initiation (in the season before harvest), flowering and early fruit development (in the current season, Table 3). Higher than average temperatures at initiation and flowering were reflected in higher Pinot noir inflorescence number per metre of row and berry number per bunch (Pinot noir and Sauvignon blanc). Berry mass was reduced (Table 3) supporting industry observations that the Marlborough 2019 harvest was in general less than anticipated (Gregan 2019). Probable environment drivers were multiple daily maximum temperatures greater than 30°C in the first six weeks of 2019. High temperature shock is reported to inhibit photosynthesis (Greer and Weston 2010) and water stress during the initial phase of berry development is reported to significantly reduce final berry mass (Ojeda et al 2001). The GFV model simulations of flowering, véraison, and harvest dates advanced since 1948 (Fig. 7) and the advances of last two seasons reflected the above average temperatures during spring (Table 3). Despite the earlier véraison and harvest dates, mean temperatures during the ripening period did not increase. (Fig. 1a), unlike increases observed elsewhere (Molitor and Junk, 2019). This possibly reflects the temperate climate of Marlborough and the abrupt changes in temperature that may occur between concurrent phenophases of vine development during the season (Figure S1).

Summerfruit

Of the four seasons' data available, September to January temperature departures from normal during 2016 – 2019 were 0.0, -0.5, +2.2 and +0.6°C. For the cherry variety, 2018 and 2019 harvest dates were 13 and 3 days respectively ahead of 2016 (a normal season). For apricots, the two heatwave summers were 14 and 2 days ahead of normal.

3.3.2 Arable

Wheat

APSIM-wheat simulations showed a reduction in grain yields during heatwave years by up to 9% compared to an estimated median historical of ~9 t/ha (Fig. 8). During heatwave years there was a more frequent occurrence of shorter cycles, earlier flowering and risk of heat stress events throughout the reproductive phase than the historical average for Lincoln.

Potatoes

The occurrence of heat and moisture stress was evident in Ohakune and Opiki (central and western North Island) and Hastings (eastern North Island) in 2017/18. In Opiki and Hastings there were supra-optimal temperatures (>25°C) for 54 and 60 days, respectively. Potato tubers from each site revealed that yield is primarily affected by the increase in the volume of unmarketable or defective tubers that reached as high as 85% of the total volume of tubers collected. This was largely due to the incidence of an array of tuber physiological defects such as enlarged lenticels, growth cracks, netting, malformations, and second growths.

For the 2018/19 season in Opiki and Hastings the number of days >25°C were 61 and 44 days (Fig.S3), respectively, with sub-optimal rainfall in Opiki (423 mm) (Table S2 in supplementary material). As a result, in Opiki and Hastings, site average harvest index, total, and marketable yield were reduced by up to 11.7%, 41.1%, and 44.8%, respectively, with reference to the cooler environment of Ohakune. The total number of tubers per plant and percentage of large- and medium-sized tubers (>50 mm) declined. Dry matter content was also down by 15.7%. The elevated temperatures in Hastings resulted in increases in plant height and leaf area, suggesting an enhanced dry matter partitioning to the haulm promoting vegetative growth (Levy and Veillux, 2007). It also increased the transpiration rate and stomatal conductance. Conversely, the water deficit in Opiki suppressed vegetative growth and stomatal conductance. These conditions led to a decrease in net photosynthesis by as much as 16.5%. The increase in the volume of unmarketable or defective tubers was dramatic (up to 44%) which significantly reduced economic yield. The defective tubers exhibited physiological defects attributed to the heat and moisture stress (Fig.S4). The most common tuber defect was second growth which came in the form of heat sprouts (in-field sprouting), chained tubers, and gemmation because of elevated soil temperatures and moisture stress (Hiller and Thornton, 2008). Second growth was most common in Hastings (18.5%) and Opiki (16.8%) with extreme heat events, and lower in Ohakune (9.7%), which is cooler.

The result of the trial showed location specific adaptations (agronomic zoning) among the tested commercial potato cultivars. Hermes performed well in the drought-prone conditions of Opiki but performance was reduced in the hotter condition of Hastings, while Snowden performed better in Hastings than in Opiki. Further analysis showed that ‘Taurus’, was the most stable and adaptable cultivar across test environments during the 2018/19 season (Fig. S5).

3.4 Marine ecosystems

Anecdotal information suggests that MHWs could be implicated in die-offs of penguins, clams, mussels and salmon (Salinger 2019a, S1) where underlying mechanisms may range from heat stress (Delorme and Sewell 2014 in S1), system-wide changes to food sources (von Biela et al 2019 in S1), to decreased resilience to pathogens (Brosnahan et al 2019 in S1). Many fish species were also observed further south than usual (S1). Dramatic losses of bull kelp (*Durvillaea* spp.) were reported immediately after the 2017/18 MHW, with 100% loss of

D. poha at Pile Bay where SST exceeded 23°C (Thomsen et al 2019, Thomsen and South 2019). Follow-up surveys showed that *Durvillaea* was also eliminated from nearby reefs. Cascading effects included losses of mussels and colonization of ephemeral seaweeds (including the invasive kelp *Undaria pinnatifida*). Furthermore, *Undaria* and other ephemeral seaweeds colonized plots that had lost *Durvillaea* in Moeraki and Oaro, respectively.

New data showed that *Durvillaea* was reduced from 100 to 40% cover in undisturbed plots in the Oaro removal experiment. Only 1.3% of the pre-MHW juvenile *Durvillaea* and no new recruits were found in disturbed plots, and *Durvillaea* were now being replaced by red and green turf algae. Furthermore, *Durvillaea* remained absent from Pile Bay and nearby reefs. Areas previously inhabited by *Durvillaea* are still dominated by *Undaria* (43% cover) in the lower zone and there was recruitment of native perennial canopy-formers (*Hormosira*, *Carpophyllum*, *Cystophora*), that were absent before the MHWs (S1).

4. Discussion and Conclusions

Heatwaves are becoming a major impact of global warming with the Intergovernmental Panel on Climate Change 5th Assessment Report (Hartmann et al 2013) indicating likely increases in unusually warm days and nights across most continents, and several occurrences of MHWs in 2019 (Blunden and Arndt 2019). The unprecedented heatwave in the 2017/18 austral summer, coupled with a combined AHW/MHW event (Salinger et al 2019a) was one of these. Although Perkins-Kirkpatrick et al (2018) suggests that the 2017/18 MHW, would have been “virtually impossible” without an anthropogenic influence, the 1934/35 event indicates a similar episode has occurred in the past in the observed record which was only 0.3°C cooler without any allowance for anthropogenic global warming (AGW). Therefore, it is very important to examine similar AHW/MHWs in the NZ region in the climate record to document drivers and impacts.

Three such austral summer events occurred – in decreasing order of magnitude 2017/18, 1934/35 and 2018/19. The last was of significance as it directly followed the 2017/18 event. These three events had AHW summer mean temperature anomalies of +2.1ºC, +1.7ºC, and +1.2ºC respectively. Indices of temperature extremes for NZ show the highest percentage of summer warm days and warm nights above the 90^{th} percentile (2017/18 33% and 29%, 1934/35 26% and 26% and 2018/19 22% and 17%) back to 1934. Counts of summer days ≥25ºC averaged 32, 22 and 26 days nationwide respectively for the three summers. For the Tasman Sea and east of NZ the three summer MHWs produced SST anomalies of +1.9 º, +1.5 º, and 1.2 ºC.

The heatwaves had very similar atmospheric and oceanic footprints, covering all the land area, the entire central and south Tasman Sea and across to 180ºE in the southwest Pacific Ocean, an area of 4 million km^2. Upper air (500-hPa) anomalies were extremely similar with very strong blocking in the Tasman Sea extending south east of NZ. The sub-surface ocean temperature, available for the latter two seasons, indicate in the GODAS profiles very shallow anomalies to the west of the South Island, with a narrow band down to about 50m in east of the South Island. The Argo float measurements averaged over the Tasman Sea confirmed surface warming from December to February, peaking between 1.5º to 3.0ºC.

Large-scale circulation anomalies showed the neutral or the La Niña phase of ENSO, and positive phase SAM for the latter two seasons. Kidson weather regimes exhibited a lack of the troughing regime. The ocean hindcast focus was on the 2017/18 and 2018/19 MHW events in the Tasman Sea. The 2017/18 event was predominantly atmospheric driven, where low wind speeds reduced the vertical mixing of heat into the water column and caused a shallow but intense surface warming. This differs with the 2018/19 case MHW where SST and mixed layer content anomalies showed similar patterns. Behrens et al (2019) notes each MHW event is unique as they are either atmospheric driven, or a combination of atmospheric surface warming and oceanic heat advection. Since 2013, above average mixed layer heat content anomalies and positive SST anomalies mean that the Tasman Sea is primed for further MHWs with supportive atmospheric circulation regardless of oceanic forcing. Trenberth et al., (2019) suggest that MHWs in the Tasman Sea region may be linked to heat transports from the South Pacific to the Indian Ocean north of Australia via the Indonesian Throughflow. Increased advection of warmer waters into the Tasman Sea is likely to be at the expense of a weak heat transport between the Pacific and Indian basins. As the inter-basin flow relaxes during El Niño years, the southward extension of the EAC is enhanced contributing to warming in the southern Tasman Sea. The dependence of heat transport between basins on ENSO conditions provides a link between the occurrence of MHWs in the Tasman Sea and the large scale oceanic and atmospheric circulation

Projected changes of pressure and wind for the late 21st century from climate models (Mullan et al 2016) show MSLP increases in the DJF period, especially to the southeast of NZ. The airflow becomes more northeasterly, and at the same time associated with more (possibly blocking) anticyclones and lacking in troughs. There is also a trend towards the SAM being more positive resulting in higher MSLPs in the NZ region, and a contraction poleward of the southern westerlies, however this depends on interplay with stratospheric ozone recovery (Arblaster et al, 2011). These are all features displayed in the 2017/18 and 2018/19 heatwaves, with circulation regimes and their analogues exhibited a lack of the troughing regime. Given that the Tasman Sea mixed layer heat content anomalies are now above average, human-induced warming has played a significant role in the latter two coupled ocean-atmospheric heatwaves.

All three heatwaves have produced significant impacts on cryosphere, terrestrial and marine ecosystems. An estimated ice loss in the small and medium glaciers have been estimated to range from 2.5 to 3.6 km^3 w.e. Between 1934/35 and 1961/62 the large glaciers had lost only about 5 km^3 w.e., as these lag in their response to climate, whereas the response of the small and medium glaciers is immediate (Chinn et al 2012). However, in the latter two heatwaves all glaciers were responding to climate warming with an accumulated ice volume loss of 17% of the 2017 volume. In contrast seasonal snowline responses are immediate. In all three the SnowSim model showed swift snowmelt commencing in mid-November and in the two hottest (2017/18 and 1934/35) heatwaves melt this was finished by 10 and 11 January respectively, the second and third earliest in simulations back to 1930. Melt rates ranged between 5.0 mm/d w.e. (2018/19) to 6.5 mm/d w.e. (1934/35) making 1934/35 the most remarkable.

Above average temperatures at inflorescence initiation and flowering resulted in higher than average inflorescence numbers, and in 2018, berry number and bunch mass for Sauvignon blanc and Pinot noir winegrapes. However, 2019 berry and bunch mass were reduced, reflecting unusually high temperatures, over 30^{o}C and vine water stress. The heat waves experienced in the past two growing seasons advanced the date of véraison and harvest but did not result in an increase in average daily temperatures during the ripening period. Harvest dates for Central Otago summer fruit were two weeks advanced in 2018 and a few days advanced in 2019 compared with normal.

In warm years, grain yields in wheat are reduced by the acceleration of crop development towards flowering and early harvest, as the crop has less time available to intercept sunlight and convert it into biomass through photosynthesis. The change in flowering date also shifts the timing when the sensitive period to heat stress occurs, illustrating the interplay of both seasonal- and threshold-type damage effects in warm years (Rezaei et al. 2015). The final crop system response depends on various additional factors, including biotic stress and farmer’s management choices such as genotype selection (Teixeira et al. 2018). Nevertheless, the general direction of yield changes suggests greater risk to spring wheat production in heatwave years. For potatoes the two heatwave years caused significant losses in the production seasons in terms of yield and tuber quality.

Major species disruptions occurred in coastal marine ecosystems where bull kelp mortalities led to local extinctions and shifts in biodiversity.

Acknowledgements

Updates of the Tasman Glacier end of summer snow line data to 1976 were provided by the late Dr Trevor Chinn. Other files from Trev were used to update the proglacial lake and downwasting of volume for the 12 large glaciers. Pascal Sirguey provided satellite imagery from the Sentinel passes for the Brewster Glacier. Jian Liu and Rob Zyskowski retrieved and prepared daily weather data to run the APSIM model. The Argo data were collected and made freely available by the International Argo Program and the national programs that contribute to it (http://www.argo.ucsd.edu, http://argo.jcommops.org). The Argo Program is part of the Global Ocean Observing System.The sub-surface temperature and SST data was collected as part of the MBIE funded Coastal Acidification: Rate, Impacts and Management (CARIM) project, provided by Kim Currie. This project obtained support through the Deep South National Science Challenge. MST was funded by the Brian Mason Trust (Impact of an unprecedented marine heatwave). PMS was funded by MBIE contract CAWX1801.

References

Arblaster JM, Meehl GA, Karoly DJ (2011). Future climate change in the Southern Hemisphere: Competing effects of ozone and greenhouse gases. Geophysical Research Letters, 38(2). https://doi.org/10.1029/2010GL045384

Behrens E, Fernandez D, Sutton P (2019) Meridional Oceanic Heat Transport Influences Marine Heatwaves in the Tasman Sea on Interannual to Decadal Timescales. Frontiers Marine Science 6: 228. https://doi.org/10.3389/fmars.2019.00228

Benthuysen J, Feng M, Zhong L (2014) Spatial patterns of warming off Western Australia during the 2011 Ningaloo Nino: quantifying impacts of remote and local forcing Cont. Shelf Res 91: 232–246. https://doi.org/10.1016/j.csr.2014.09.014

Blunden J, Arndt DS (2019) A Look at 2018 Takeaway Points from the State of the Climate 2018 Supplement. Bull. Amer. Met Soc September 2019 1527 – 1538. https://doi.org/10.1175/BAMS-D-19-0193.1

Chinn, TJ (2001) Distribution of the glacial water resources of New Zealand. Journal of Hydrology (New Zealand) 40 (2): 139–187. https://www.jstor.org/stable/43922047.

Chinn TJ, Fitzharris BB, Salinger MJ, Willsman A (2012) Annual ice volume changes 1976–2008 for the New Zealand Southern Alps. Glob Planet Change 92–93: July 2012 105-118. https://doi.org/10.1016/j.gloplacha.2012.04.002

Compo, G. P., Whitaker, J. S., Sardeshmukh, P. D., Matsui, N., Allan, R. J., Yin, X., . . . Worley, S. J. (2011). The Twentieth Century reanalysis project. Quarterly Journal of the Royal Meteorological Society, 137(654): 1-28. https://doiorg/10.1002/qj.776

Dee DP, Uppala SM, Simmons AJ, Berrisford P, Poli P, Kobayashi S, . . . Vitart F (2011). The ERA-Interim reanalysis: configuration and performance of the data assimilation system. Quarterly Journal of the Royal Meteorological Society, 137(656): 553-597. https://doi.org/10.1002/qj.828

de Lautour S (1999) “The climatology of seasonal snow”. MSc Thesis, Department of Geography, University of Otago.

Fitzharris B, Garr GE (1995) Simulation of past variability in seasonal snow in the Southern Alps, New Zealand. Annals of Glaciology 21: 377-382. https://doi.org/10.3189/S0260305500016098

Garr CE, Fitzharris BB (1996) Using seasonal snow to forecast inflows into South Island hydro lakes. In: Prospects and Needs for Climate Forecasting, The Royal Society of New Zealand Miscellaneous Series 34: 63-67 [ISBN 0-908654-61-8]

Gong D, Wang S (1999) Definition of Antarctic oscillation index. Geophysical Research Letters 20 (4): 459-462. https://doi.org/10.1029/1999GL900003

Gordon ND (1986) The Southern Oscillation and New Zealand weather. Monthly Weather Review 114: 371-387. https://doi.org/10.1175/1520-0493(1986)114<0371:TSOANZ>2.0.CO;2

Greer DH, Weston C (2010) Heat stress affects flowering, berry growth, sugar accumulation and photosynthesis of *Vitis vinifera* cv. Semillon grapevines grown in a controlled environment. Functional Plant Biology 37: 206-214. https://doi.org/10.1071/FP09209

Gregan, P 2019. Vintage 2019 small but stunning. https://www.nzwine.com/media/13040/vintage-2019-small-but-stunning.pdf

Hartmann DL, Klein Tank AMG, Rusticucci M, Alexander LV, Brönnimann S, Charabi Y, Dentener FJ, Dlugokencky EG, Easterling DR, Kaplan A, Soden BJ, Thorne PW, Wild M, Zhai PM (2013) Observations: Atmosphere and Surface. In: Climate Change 2013: The Physical Science Basis. Contribution of Working Group I to the Fifth Assessment Report of the Intergovernmental Panel on Climate Change [Stocker TF, Qin D, Plattner K-G, Tignor M, Allen SK, Boschung J, Nauels A, Xia Y, Bex V, Midgley PM (eds.)]. Cambridge University Press, Cambridge, United Kingdom and New York, NY, USA.

Heidemann H, Ribbe J (2019) Marine Heat Waves and the Influence of El Niño off Southeast Queensland, Australia, Frontiers of Marine Science, 20 February 2019. https://doi.org/10.3389/fmars.2019.0005d

Henley BJ, Gergis J, Karoly DJ, Power SB, Kennedy J, Folland CK (2015). A Tripole Index for the Interdecadal Pacific Oscillation. Climate Dynamics 45 (11-12): 3077-3090. http://dx.doi.org/10.1007/s00382-015-2525-1 . Accessed on 05 27 2019 at https://www.esrl.noaa.gov/psd/data/timeseries/IPOTPI.

Hiller L, Thornton RE (2008). Managing Physiological Disorders. Chapter 23: 235-246.In D. A. Johnson (Ed.), Potato Health Management Second Edition. Minnesota, USA: APS Press. ISBN 978-0-89054-353-5.

Hobday A, Alexander LV, Perkins SE, Smale DA, Straub SC, Oliver ECJ, Benthuysen JA, Burrows MT, Donat MG, Feng M, Holbrook NJ, Moore PJ, Scannell HA, Sen Gupta A, Wernberg T (2016) A hierarchical approach to defining marine heatwaves Prog. Oceanogr 141: 227–238.

https://doi.org/10.1016/j.pocean.2015.1012.1014. Outcome of Workshop #1.

Holzworth DP, Huth NI, deVoil PG, ZurcherEJ, Herrmann NI, McLean G, Chenu K, van Oosterom EJ, Snow V, Murphy C, Moore AD, Brown H, Whish J.M, Verrall S, Fainges J, Bell LW, Peake AS, Poulton PL, Hochman Z, Thorburn PJ, Gaydon DS, Dalgliesh NP, Rodriguez D, Cox H, Chapman S, Doherty A, Teixeira E, Sharp J, Cichota R, Vogeler I, Li FY, Wang E, Hammer GL, Robertson MJ, Dimes JP, Whitbread AM, Hunt J, van Rees H, McClelland T, Carberry PS, Hargreaves JNG, MacLeod N, McDonald C, Harsdorf J, Wedgwood S, Keating BA (2014) APSIM -

Evolution towards a new generation of agricultural systems simulation. Environmental Modelling Software 62. https://doi:10.1016/j.envsoft.2014.07.009

Jayne SR, Roemmich D, Zilberman N, Riser SC, Johnson KS, Johnson KC,Piotrowicz SR 2017 The Argo Program: present and future, Oceanography 30: 18–28. https://doi.org/10.5670/oceanog.2017.213

Kidson E (1935) The summer of 1934/35 in New Zealand NZ Met.Office Note 16 12pp

Kidson JW (2000) An analysis of New Zealand synoptic types and their use in defining weather regimes. International Journal of Climatology 20 (3): 299-315. https://doi.org/10.1002/(SICI)1097-0088(20000315)20:3<299::AID-JOC474>3.0.CO;2-B

Kistler R, Collins W, Saha S, White G, Woollen J, Kalnay E, . . . Fiorino M. (2001). The NCEP–NCAR 50–year reanalysis: Monthly means CD–ROM and documentation. Bulletin of the American Meteorological Society, 82(2): 247–268. https://doi.org/10.1175/1520-0477(2001)082<0247:TNNYRM>2.3.CO;2

Levy D, Veilleux RE (2007) Adaptation of potato to high temperatures and salinity - A Review. Amer J of Potato Res 84: 487-506. https://doi.org/10.1007/BF02987885

Molitor D, Junk J (2019) Climate change is implicating a two-fold impact on air temperature increase in the ripening period under the conditions of the Luxembourgish grapegrowing region. Oeno-one 3: 409-422. https://doi.org/10.20870/oeno-one.2019.53.3.2329

Mullan AB, Stuart SJ, Hadfield MG, Smith MJ (2010) Report on the Review of NIWA's 'Seven-Station' Temperature Series NIWA Information Series No. 78. 175 pp. https://www.niwa.co.nz/sites/niwa.co.nz/files/import/attachments/Report-on-the-Review-of-NIWAas-Seven-Station-Temperature-Series_v3.pdf

Mullan AB, Sood A, Stuart S (2016) Climate Change Projections for New Zealand: Atmosphere Projections Based on Simulations from the IPCC Fifth Assessment Wellington: Ministry for the Environment. https://www.mfe.govt.nz/sites/default/files/media/Climate%20Change/Climate-change-projections-2nd-edition-final.pdf

Ojeda H, Deloire A, Carbonneau A (2001) Influence of water deficits on grape berry growth. Vitis 40: 141-145. https://www.researchgate.net/publication/285702011_Influence_of_water_deficits_on_grape_berry_growth

Oliver ECJ, Benthuysen JA, Bindoff NL, Hobday AJ, Holbrook NJ, Mundy CN, Perkins-Kirkpatrick SE (2017) The unprecedented 2015/16 Tasman Sea marine heatwave. Nature Communications 8. https://doi.org/10.1038/ncomms16101

Oliver ECJ, Donat MG, Moore PJ, Smale DA, Alexander LV, Benthuysen JA, Feng M, Gupta AS, Hobday AJ, Holbrook NJ, Perkins-Kirkpatrick SE, Straub SC, Wernberg T (2018) Longer and more frequent marine heatwaves over the past century. Nature Communications 9: 1324. https://doi.org/10.1038/s41467-018-03732-9

Parker A, Garcia de Cortazar-Atauri I, Chuine I, Barbeau G, Bois B, Boursiquot J-M, Cahurel J-Y, Claverie M, Dufourcq T, Geny L, Guimberteau G, Hofmann RW, Jacquet O, Lacombe T, Monamy C, Ojeda H, Panigai L, Payan J-C, Lovelle BR, Rouchaud E, Schneider C, Spring J-L, Storchi P, Tomasi D, Trambouze W, Trought M and van Leeuwen C (2013) Classification of varieties for their timing of flowering and véraison using a modelling approach: A case study for the grapevine species *Vitis vinifera* L. Agricultural and Forest Meteorology 180: 249-264. http://dx.doi.org/10.1016/j.agrformet.2013.06.005

Parker AK (2012) Modelling phenology and maturation of the grapevine *Vitis vinifera* L.: Varietal differences and the role of leaf area to fruit weight ratio manipulations Lincoln University PhD thesis Lincoln University

Perkins-Krikpatrick SE, King SE, Cougnon AD, Grosese EA, Oliver MR, Holbrook NJ, Lewis SC Pourasghar F (2018) The role of natural variability and anthropogenic climate change in the 2017/18 Tasman Sea marine heatwave. Bulletin of American Meteorological Society http://doi.org/10.1175/BAMS-D-18-0116.1

Rezaei EE, Siebert S Ewert F (2015) Intensity of heat stress in winter wheat—phenology compensates for the adverse effect of global warming. Environmental Research Letters 10 (24012). https://doi.org/10.1088/1748-9326/10/2/024012

Rykaczewska K (2017) Impact of heat and drought stresses on size and quality of the potato yield. Plant Soil Environ 63(1): 40-46. https://doi.org/10.17221/691/2016-PSE

Saha S et al (2006) The NCEP climate forecast system. Journal of Climate 19: 3483–3517. https://doi.org/10.1175/JCLI-D-12-00823.*1*

Salinger M J (1979) New Zealand climate: the temperature record, historical data and some agricultural implications. Climatic Change 2: 109-126. https://doi.org/10.1007/BF00133218

Salinger MJ, McGann RP, Coutts L, Collen B, Fouhy E (1992) South Pacific historical climate network. Temperature trends in New Zealand and outlying islands, 1920-1990. New Zealand Meteorological Service, 46pp, Wellington. ISBN 0-477-01598-0.

Salinger MJ, Renwick JA, Behrens E, Mullan AB, Diamond HJ, Sirguey P, Smith RO, Trought MCT, Alexander LV, Cullen NC, Fitzharris BB, Hepburn CD, Parker AK, Sutton PJ (2019a) The unprecedented coupled ocean-atmosphere summer heatwave in the New Zealand region 2017/18: Drivers, mechanisms and impacts. Environmental Research Letters 14 (4): https://doi.org/10.1088/1748-9326/ab012a

Salinger MJ, Chinn TJ, Fitzharris BB (2019b) Annual ice volume changes 1949 –2019 for the New Zealand Southern Alps. International Journal of Climatology (submitted).

Smale DA, Wernberg T, Oliver ECJ, Thomsen M, Harvey BP, Straub SC, Burrows MT, Alexander LV, Benthusen JA, Donat M, Feng M, Perkins-Kirkpatrick SE, Scannell HA, Sen Gupta A, Payne BL, Moore PJ (2019) Marine heatwaves threaten global biodiversity and the provision of ecosystem services. Nature Climate Change 9: 306–312 https://doi.org/10.1038/s41558-019-0412-1

Siano AB, Roskruge N, Kerchkhoffs LHJ, Sofkova-Bobcheva S (2018) Yield and tuber quality variability in commercial potato cultivars under abiotic stress in New Zealand. Agronomy New Zealand 48: 149 – 163. https://www.agronomysociety.nz/files/ASNZ_2018_14._Potato_yield_and_tuber_quality.pdf

Sutton PJ, Bowen M (2019) Ocean temperature change around New Zealand over the last 36 years. New Zealand Journal of Marine and Freshwater Research 53 (3): 305-326. https://doi.org/10.1080/00288330.2018.1562945

Teixeira, EI, de Ruiter J, Ausseil A-GA-G, Daigneault A, Johnstone P, Holmes A, Tait A, Ewert F (2018) Adapting crop rotations to climate change in regional impact modelling assessments. Sci. Total Environ. 616–617, 785–795. https://doi.org/10.1016/j.scitotenv.2017.10.247

Thompson, D. W. J., Solomon, S., Kushner, P. J., England, M. H., Grise, K. M., & Karoly, D. J. (2011). Signatures of the Antarctic ozone hole in Southern Hemisphere surface climate change. *Nature Geoscience*, *4*(11), 741-749. https://doi.org/10.1038/NGEO1296

Thomsen MS, Gerrity S, Alestra T, South PM, Lilley S, Monstrani L, Schiel DR (2019) Local extinction of bull kelp (Durvillaea spp.) due to a marine heatwave. Frontiers Marine Science 6: 84.

Thomsen MS, South P (2019) Communities and attachment networks associated with primary, secondary and alternative foundation species; a case of stressed and disturbed stands of Southern Bull Kelp. Diversity 11(4): 56.

Trenberth KE (1976) Fluctuations and trends in indices of the southern hemispheric circulation. Quart. J. Roy. Met. Soc. 102 (431): 65-75. https://doi.org/10.1002/qj.4971024310

Trenberth KE, Zhang Y, Fasullo JT, Cheng L (2019) Observation-Based Estimates of Global and Basin Ocean Meridional Heat Transport Time Series. *Journal of Climate 32*, 4567-4583. https://doi.org/10.1175/JCLI-D-18-0872.1

Thomsen MS, Mondardini L, Alestra T, Gerrity S, Tait L, South PM, Lilley SA, Schiel DR (2019) Local Extinction of Bull Kelp (Durvillaea spp.) due to a Marine Heatwave Frontiers in Marine Science 6 March 2019. https://doi.org/10.3389/fmars.2019.00084

Trought MCT (2005) Fruitset - possible implications on wine quality. In: Garis Kd, Dundon, C., Johnstone, R. and Partridge, S., ed, Transforming flowers to fruit. Mildura, Australia: Australian Society of Viticulture and Oenology, 32-36.

Troup AJ (1965) The ‘southern oscillation’. Quart. J. Roy. Met. Soc. 91 (390): 490-506 https://doi.org/10.1002/qj.49709139009

Table 1. Indices for the three heatwaves. NZ22T is the 22 station NZT series for surface temperature, ERSST is the ERSST version 5 for the New Zealand (NZ) Exclusive Economic Zone, and NZEEZT are NZ22T and ERSST combined and weighted for the entire NZ region. SAM the Southern Annular Mode (Gong and Wang (1998), SOI the Troup (1965) Southern Oscillation Index, and the Interdecadal Pacific Oscillation (IPO) the tripolar index (Henley et al 2015), Z1 and M1 are Trenberth (1976) zonal and meridional indices. Kidson regimes are Trough, Zonal and Block anomalies (Kidson 2000). TX90p and TN90p are the percentages of days above the maximum (TX) and minimum (TN) daily 90 percentile temperatures, with Days ≥25ºC counts ≥25ºC, all averaged for 26 NZ climate stations.

Metric	1934/35	2017/18	2018/19
NZ22T	1.73	2.07	1.21
ERSSTv5	1.46	1.92	1.15
NZEEZ	1.48	1.92	1.15
SAM	-1.21	1.76	0.36
SOI	-1	7	74
IPO	-0.16	-0.92	0.09
Z1	-16	-15	-7
M1	-40	8	-5
Kidson Trough		2	3
Kidson Zonal		-9	4
Kidson Block		8	-7
Warm days TX90p	26	33	22
Warm nights TN90p	26	29	17
Days ≥25ºC	22	32	26

Tables 2 a-c. Detailed 500-hPa Analogue Results by Season. These are the results of an analysis of the atmospheric circulation patterns were compared using anomaly correlation and root mean-square difference over the region 135°E-140°W, 65°S-25°S (see text) compared to a. 1934/35 b. 2017/18 and c. 2018/19 season. Bolded are significant (p<0.05) for SAM and SOI (x10), and 10 or 90 percentiles for Z1, M1 and Kidson regimes.

Season	**SAM Value**	**SOI Value**	**Z1 Value**	**M1 Value**	**Trough**	**Kidson Zonal**	**Block**
OND 1915	-1.37	-2	12	-28			
JFM 1935	-2.22	4	**-10**	**-35**			
FMA 1935	**-3.12**	3	**-23**	**-35**			
SON 1965	0.01	-16	-15	-9	1	13	-14
JFM 1966	-1.83	-12	-5	-23	-3	-7	10
AMJ 1978	-1.06	4	**-40**	**-10**	**11**	**-7**	**-4**
JJA 1979	1.45	-3	-14	-34	-16	6	11
NDJ 1981	0.59	5	**13**	**-20**	**1**	**-8**	**7**
AMJ 2003	0.50	-9	3	-12	-7	3	5
Mean Value	-1.21	-1	-9	-23	-2	0	3
DJF 1935	-1.08	-3	-16	**-40**			

Season	**SAM Value**	**SOI Value**	**Z1 Value**	**M1 Value**	**Trough**	**Kidson Zonal**	**Block**
JJA 1979	1.45	-3	-14	-34	-10	3	7
OND 1981	0.63	-1	11	-35	**-13**	2	11
JJA 1985	0.66	-2	**-3**	-33	-5	-3	8
DJF 1994	1.04	-1	**1**	-37	-4	-2	
FMA 1999	1.36	12	8	-35	**-13**	-9	**22**
MAM 1999	2.03	10	-3	-41	**-18**	7	**11**
JAS 2005	0.48	-2	8	-10	-10	9	1
DJF 2008	**1.78**	**17**	-19	-22	-10	**-11**	**21**
DJF 2013	-0.05	-8	1	0	-6	5	1
JFM 2018	1.48	**45**	-10	0	1	**-11**	10
Mean Value	1.09	7	-4	-20	-11	-1	10
DJF 2018	**1.76**	7	-15	8	2	**-9**	8

Season	**SAM Value**	**SOI Value**	**Z1 Value**	**M1 Value**	**Trough**	**Kidson Zonal**	**Block**
JFM 1982	133	3	**12**	-15	1	-3	6
JJA 1993	**1.49**	-16	**18**	-33	**-13**	**21**	-8
DJF 1995	1.14	-8	**-14**	9	**-15**	**11**	4
AMJ 1999	**1.40**	7	-6	1	**-11**	7	4
MJJ 1999	1.60	2	0	45	**-13**	**16**	-3
DJF 2013	-0.05	-8	1	-22	-6	5	1
NDJ 2015	1.17	-22	**-7**	3	-10	3	7
DJF 2016	1.37	-33	-5	1	-10	5	5
FMA 2016	**2.25**	-32	1	**-38**	**-15**	**-17**	-2
NDJ 2018	2.36	**29**	**-17**	-24	0	6	-6
Mean Value	1.31	-8	-2	-7	-9	9	1
DJF 2019	0.36	**74**	-7	-5	3	4	-7

Table 3. Key phenological stages, temperature and yield data. a. Timing of key phenological stages and temperatures at and between those stages, and b. Sauvignon blanc and Pinot noir yield component data.

	Date			**Mean daily temperature at key phenology times(ºC)**		**Mean daily temperature between key phenology times (ºC)**		
Harvest year	flowering	véraison	20ºBrix	Initiation*	Flowering*	1 Sept to flowering	Flowering to véraison	Véraison to 20ºBrix
Long-term average (1987-2017)	5 Dec	15 Feb	21 Mar	17.6	17.3	12.9	17.7	16.9
2018	30 Nov	2 Feb	5 Mar	17.9	18.6	13.6	19.7	19.0
2019	2 Dec	6 Feb	12 Mar	18.7	18.5	13.3	19.1	17.6

*Note: initiation temperatures occur in the season before harvest, flowering temperatures are in the season of harvest. Dates used to estimate temperatures at this time are Dec 14 to Jan 17 and Dec 9 to Jan 9 for initiation and flowering respectively (Trought 2005) 17 and Dec 9 to Jan 9 for initiation and flowering respectively (Trought in S1)

	Average (2010-19)	**Cv* 2010-2019**	**Vintage 2018**	**Vintage 2019**
Pinot noir				
Average bunch mass (g)	113.8	25.0	131.9 (6.5)**	76.4 (4.2)
Average berry mass (g)	1.50	13.02	1.85 (0.04)	1.19 (0.02)
Average berry number per bunch	39.6	13.37	46.5 (3.5)	38.9 (3.1)
Inflorescence number per m row	24.4	19.7	25.9 (0.8)	28.1 (0.7)
Sauvignon blanc				
Average bunch mass (g)	144.4	16.3	183.4 (3.58)	131.3 (3.63)
Average berry mass (g)	2.05	8.15	2.37 (0.03)	1.78 (0.04)
Average berry number per bunch	70.9	12.7	78.2 (1.3)	74.9 (2.4)
Inflorescence number per m row	29.3	14.0	29.3 (0.6)	30.0 (0.8)

**cv = coefficient of variation ** numbers in brackets are the standard error of the mean*

Figure

Figure 1. a. New Zealand 22 station temperatures (red smoothed), b. Extremes – TX90p, TN90p and days >25°C, c. Tasman Sea SST, d-f. SST DJF. d. 1934/35, e. 2017/18 and f. 2018/19

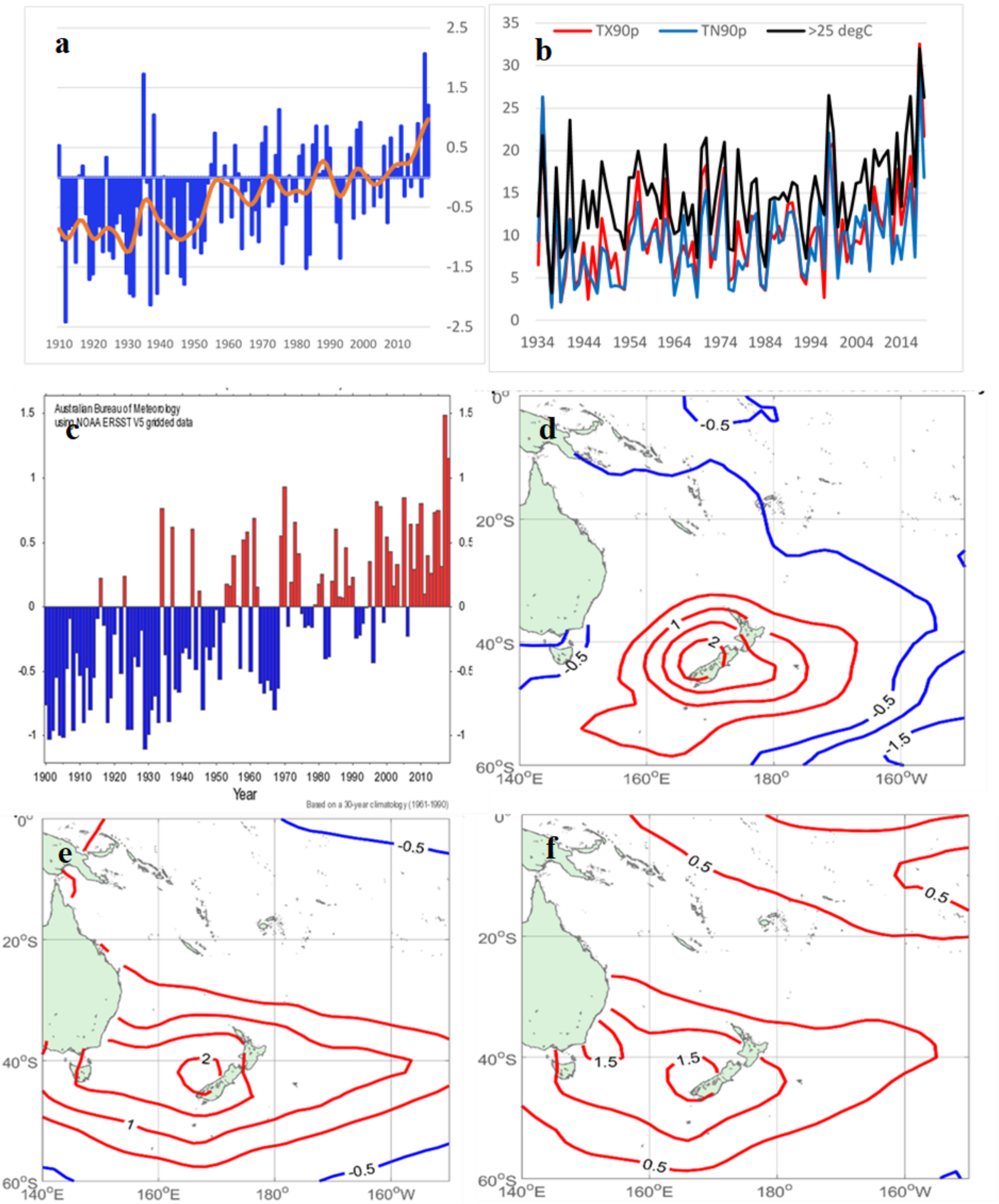

Figure. 2. (First row). Time series of sea surface temperature (SST) climatology (1981-2011; blue), 90th percentile MHW threshold (orange) and summer 2017/18 to 2018/19 SSTs (black) from the (a) eastern Tasman Sea (160-172°E, 35-45°S) and (b) the Portobello Marine Laboratory (45.88°S, 170.5°E) The red shaded regions identify periods associated with MHWs from each location using the Hobday et al. (2016) definition. 0°E). The red shaded regions identify periods associated with MHWs detected in the SST time series from each location using the Hobday et al. [2016] definition. (Second row). The duration of each MHW detected in the SST time series for the (c) eastern Tasman Sea and (d) Portobello Marine Laboratory. The red shaded region highlights MHWs detected between October 2017 and July 2019. (Third row). As above but showing the maximum intensity of each MHW detected in the SST time series for (e) the eastern Tasman Sea and (f) Portobello Marine Laboratory.

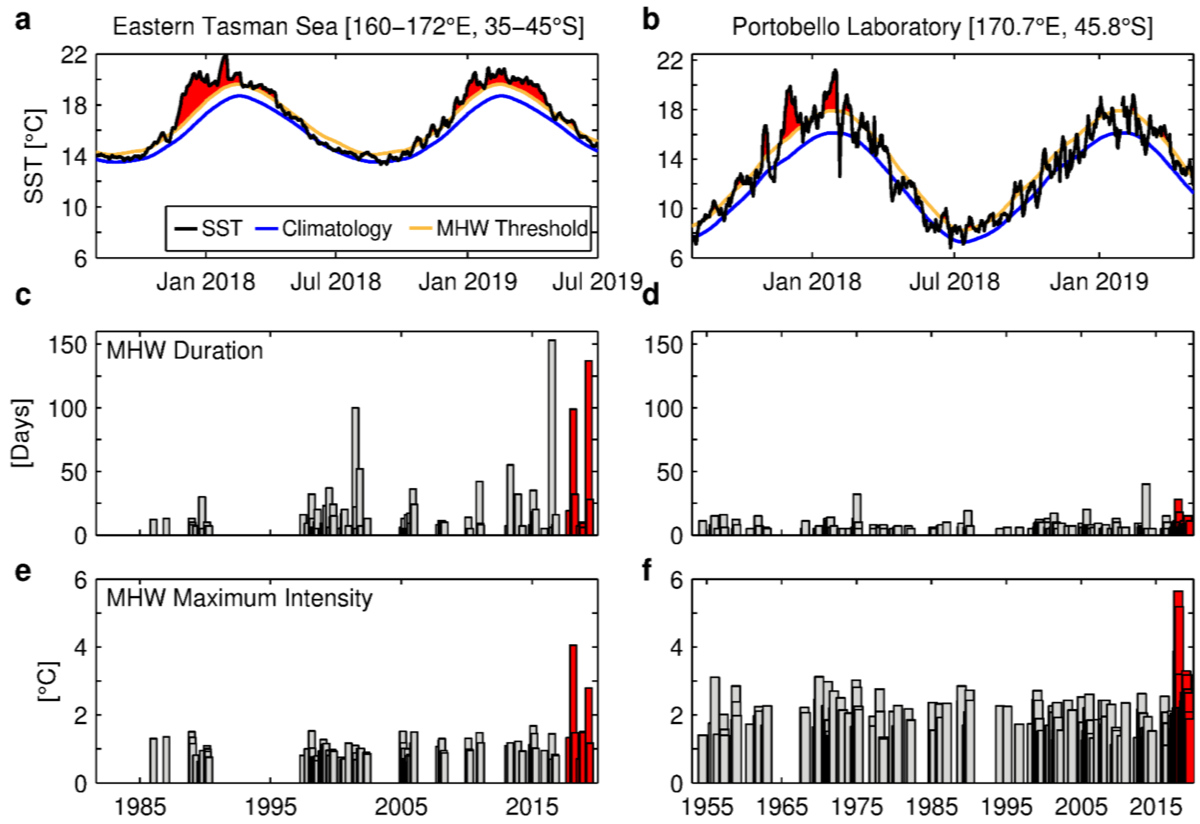

Figure 3. Atmospheric circulation. a-c. DJF mean sea level pressure anomaly. a. 1934/35, b. 2017/18 and c. 2018/19. d-f 500 hPa anomaly. d. 1934/35, e. 2017/18, and f. 2018/19.

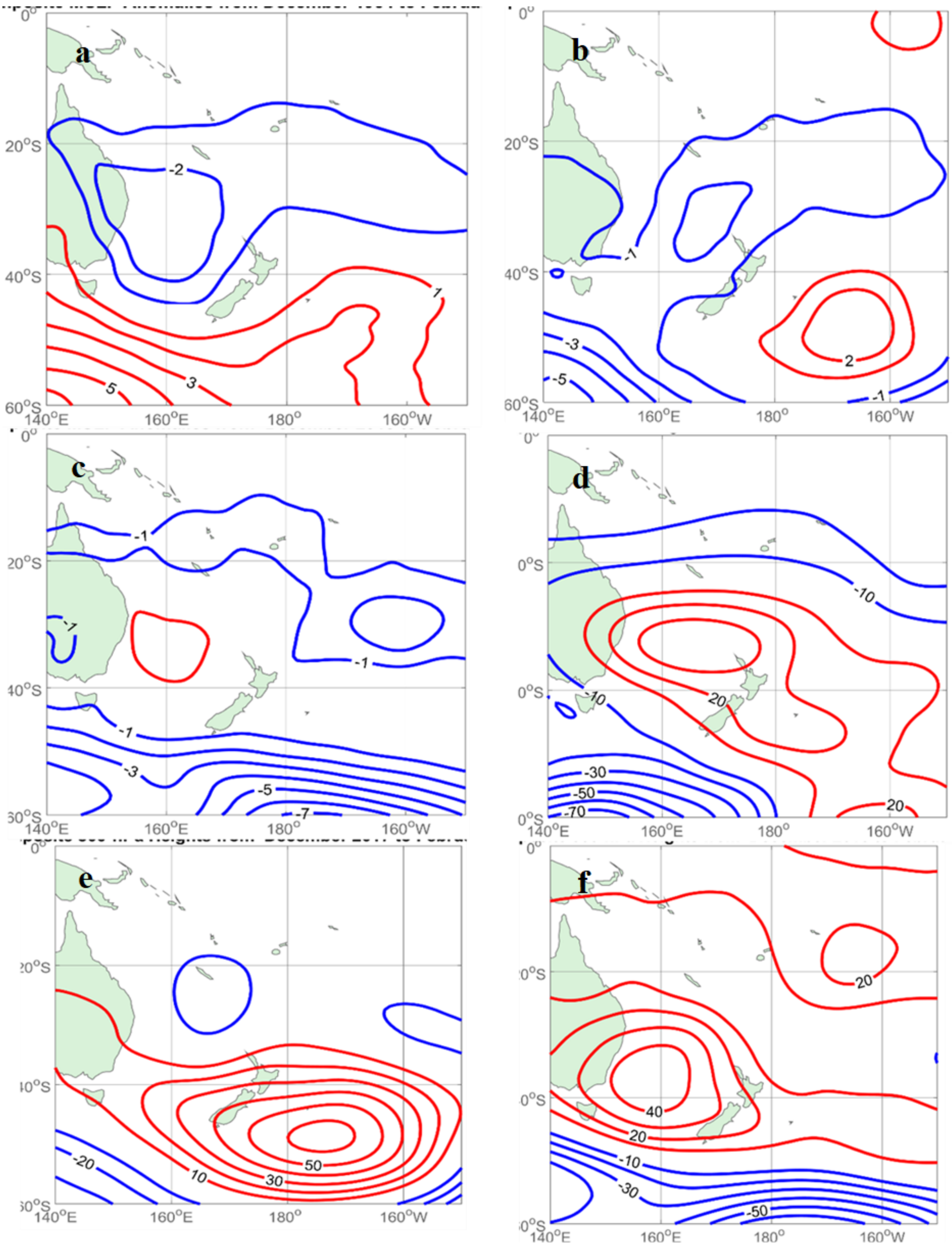

Figure 4. Subsurface sea temperature anomalies. a and b. GODAS subsurface Tasman Sea. a. DJF 2017/18 and b. DJF 2018/19. c. Subsurface temperature anomalies in the eastern Tasman Sea from Argo floats January 2017 – April 2019.

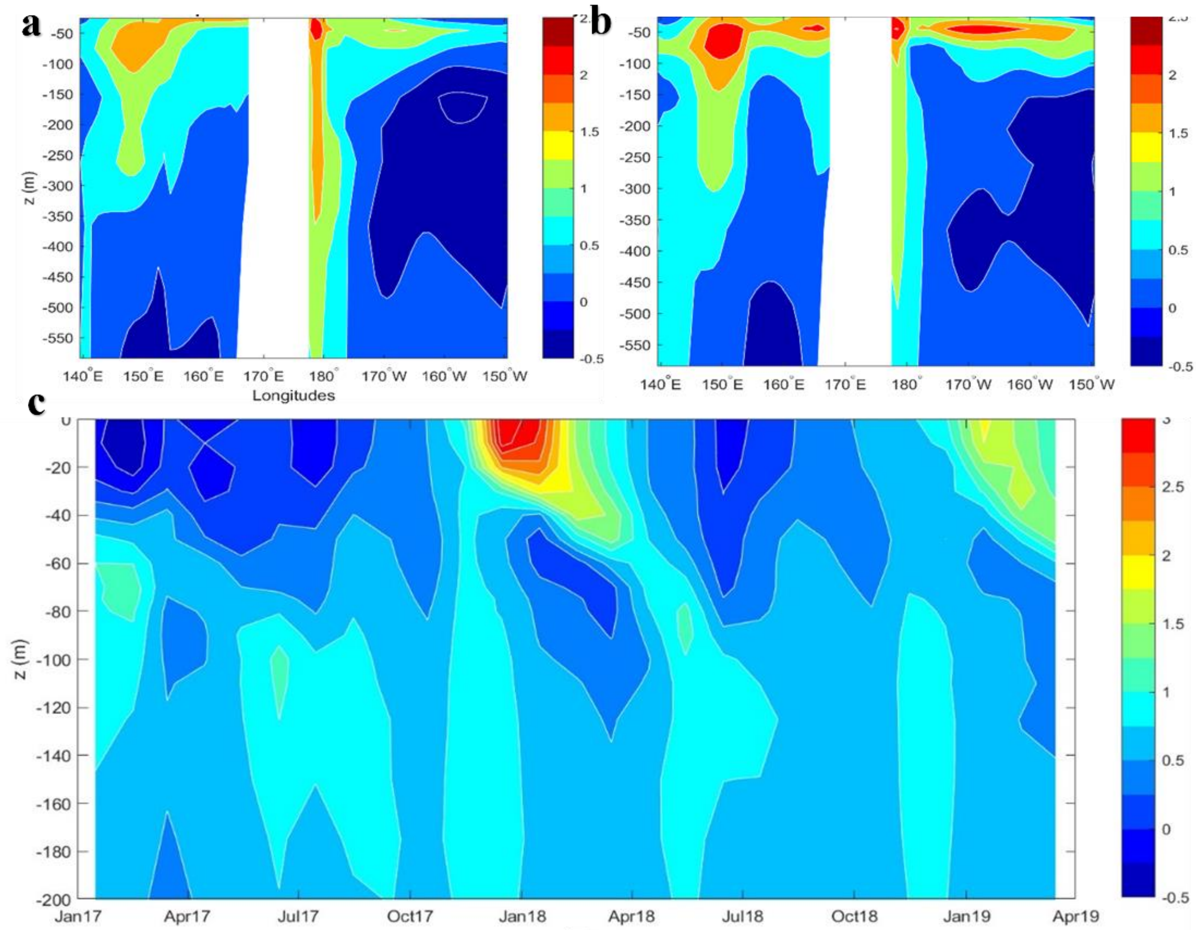

Figure 5. Modelled SST anomalies (a-c) for November-December 2015, 2017 and 2018 in °C. The white contour lines show the mixed layer depths with 10 m intervals. Mixed layer heat content anomaly (d-f) for the same period in J. (g) Timeseries of integrated or averaged anomalies over the Tasman Sea between 145°E, 175°E, 50°S, 30°S) for November-December. Grey, red and blue bars show integrated mixed layer heat content anomalies, average SST anomalies, and average wind speed anomalies, respectively.

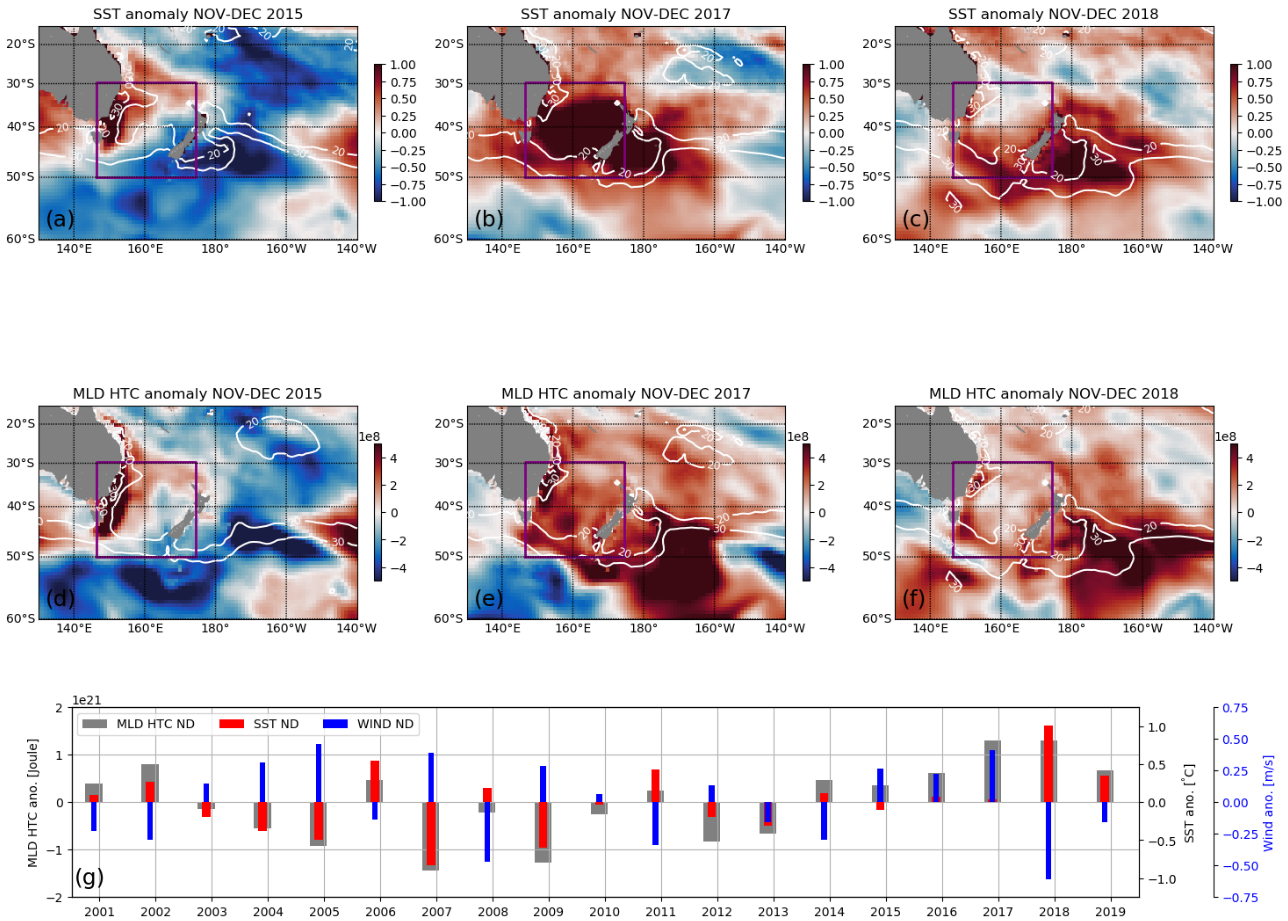

Figure 6. Southern Alps ice volume and seasonal snow. a. Southern Alps ice volume change (km^3 of water equivalent), between years, for all glaciers of the Southern Alps from 1962 to 2019. b-c. Estimated water stored as seasonal snow (mm) from SnowSim for the period 1987 – 2019.

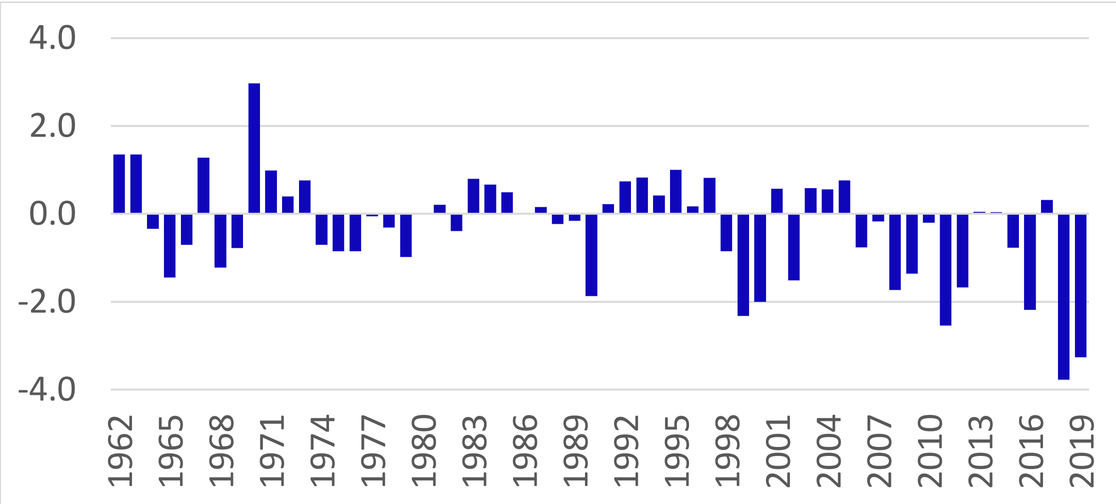

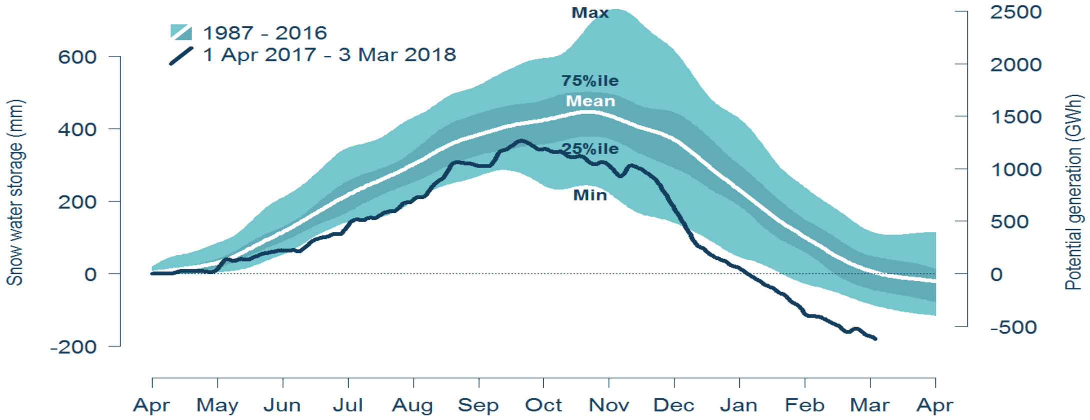

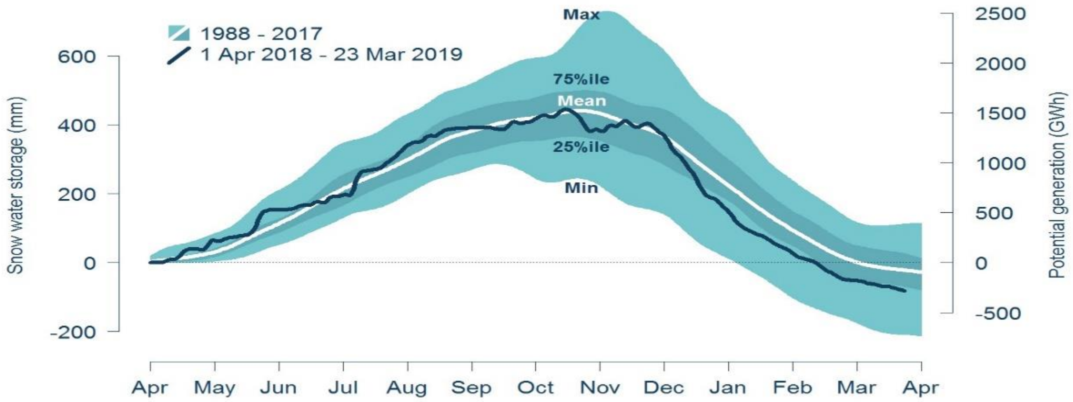

Figure 7. Predicted Marlborough Sauvignon blanc (a) flowering, (b) véraison, (c) 20°Brix dates using GFV phenology model (Parker et al. 2013). (d) mean daily temperature during ripening véraison to 20°Brix. The fitted lines are (a) y=228.4-0.065x, R_2 0.124; (b) y=371-0.101x, R_2 0.141; (c) y= 418-0.107x, R_2 0.096; (d) y=19.56-0.0013x, R_2 0.0005. Note: the late phenology in 1993 coincided with the Mt Pinatubo volcanic eruption.

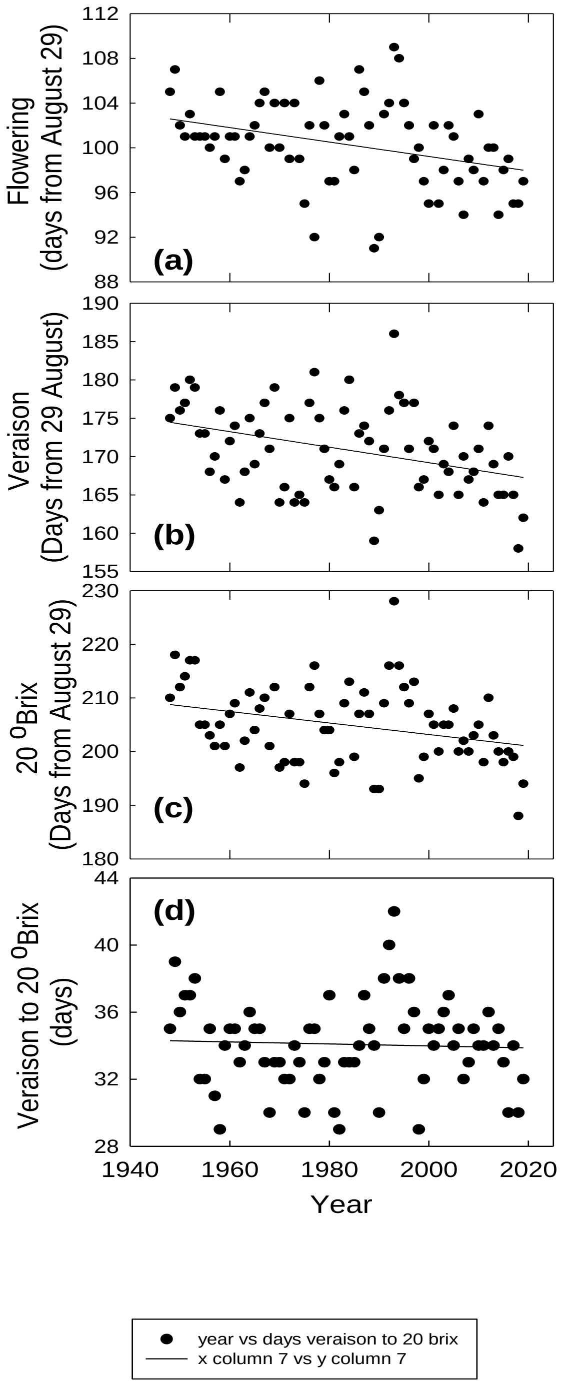

Figure 8._Simulated physiological responses of irrigated spring wheat during three heatwave years (1934/35, 2017/18 and 2018/19) in Lincoln, Canterbury, New Zealand. Dashed lines are the median (black) and average (dark-grey) of 30 years (1981-2010).